*Journal of Advanced Ceramics*
2012, 1(3): 241-248
DOI: 10.1007/s40145-012-0023-z ISSN 2226-4108

**Research Article**

# Effect of equiproprotional substitution of Zn and Mn in $BaTiO_3$ ceramic—An index to multiferroic applications

S. K. DAS, P. P. ROUT, S. K. PRADHAN, B. K. ROUL*

*Institute of Materials Science, Planetarium Building, Acharya Vihar, Bhubaneswar 751013, India*

Received: September 22, 2012; Accepted: October 9, 2012


**Abstract:** This paper reports that ferromagnetism (FM) can be induced in ferroelectric barium titanate ($BaTiO_3$) ceramic with selection of appropriate substituents like Zn and Mn. High density polycrystalline samples of Zn and Mn substituted $BaTiO_3$ ($Ba_{1-x}Zn_xTi_{1-x}Mn_xO_3$, $x$=0, 0.02, 0.04, 0.06, 0.08 and 0.1) were prepared using slow step solid state sintering technique to study the effect of equiproprotional substituents on structural, ferroelectric and magnetic properties of $BaTiO_3$ (BTO). High precision electrical and magnetic measurements were carried out along with XRD, XPS, and SEM to understand and co-relate magnetic and ferroelectric hysteresis loop observed at room temperature with different values of '$x$'. It is seen that ferroelectric hysteresis loop (P~E) is deteriorated (became lossy type) with the increase of Zn and Mn concentration. However, at $x$=0.1, the material showed the signature of room temperature ferromagnetism, which is an index for BTO to became a promising material for multiferroic applications. M~H loops observed in Zn and Mn substituted BTO are expected to be due to the formation of oxygen vacancies and exchange interaction induced magnetism.

**Key words:** ceramic; magnetism; hexagonal; polarization

## 1 Introduction

The research and development activities of multiferroic materials have been increasing many fold during recent years for its potential applications in many upcoming broad areas of spintronics, magneto-electrics and magnetic semiconductors. As known, multiferroic materials possess more than one type of ferroic order such as ferromagnetic/ antiferromagnetic, ferroelectric, ferroelastic and ferrotoroidics. This class of materials finds promising applications in nonvolatile memory, memory-cell capacitor, electromagnetic-interference filter, sensors and so forth. Basically, multiferroic materials have been synthesized by means of two routes. One is the composite/combination of a ferroelectric material with a ferromagnetic material [1] and second one is the doping of magnetic impurities into a ferroelectric material [1]. Most of the ferroelectric materials studied for multiferroic applications are of $ABO_3$ (where A= rare earth or alkaline earth element and B=transition element) type oxides. $BaTiO_3$ (BTO), which is a promising $ABO_3$ type of ferroelectric have been proven both theoretically and experimentally to be a multiferroic [1-4]. BTO undergoes three well-known

* Corresponding Author.
E-mail: ims@iopb.res.in

structural phase transitions: Cubic to tetragonal at 403 K [5], tetragonal to orthorhombic at 278 K [5], and orthorhombic to rhombohedral at 183 K [5]. In addition to these phases, it has been reported that hexagonal structured $BaTiO_3$ (h-BTO) is stable above 1460 ℃ [6]. It is also established that doping with 3d ions such as Mn, Fe or Ni gives rise to the development of h- BTO at room temperature [6,7].

The properties of BTO change drastically with the type and concentration of metal ions substituted in the lattice and dependent on the processing conditions [7-10]. The transition metal ions in BTO ceramics are of special interest as they can induce magnetism in BTO [8-12]. Dang *et al* [1] showed that room temperature ferromagnetic order exists in $BaTi_{1-x}Fe_xO_3$. The ferromagnetic behavior was observed in $Ba_xTi_{0.95}Mn_{0.05}O_3$ ($x$=1, 1.1, 1.2) at low temperature and the nominal ratio of Ba/Ti has a great influence on the ferromagnetic properties [3]. In order to improve the functional qualities and extend the areas of application of barium titanate, different elements have been used as dopants in A or B site [8]. Zinc (with an ionic radius of 0.74 Å) can either be substituted for Ba or Ti in BTO as the ionic radius of Ba is 1.35 Å and that of Ti is in the range of 0.605 Å to 0.67 Å [13,14]. The ionic radius of Mn is in the range of 0.53 Å to 0.83 Å [14]. It can only be substituted in B site of BTO [14]. Earlier reports [10,12] showed that induction of magnetism in BTO sharply deteriorates its ferroelectricity. Theoretical calculation of Kaoru Miura *et al* [15] showed that Coulomb repulsions between Ti 3s and 3p states and O 2s and 2p states have an important role for the appearance of Ti ion displacement, which causes ferroelectricity in BTO. Again, Zn-O Coulomb repulsion is stronger than that of Ti-O Coulomb repulsions due to 3s, 3p, and 3d (d10) states of the Zn ion [15]. The Coulomb repulsions play important role for the occurrence of ferroelectricity [15]. The above facts inspire us to take 'Zn' as substituent instead of other transition group elements. It is also reported that magnetism is induced in BTO by doping of Mn [2,3]. Considering the above reports, we have equiproprotionally co-doped Zn and Mn metal ions into BTO system in order to find their mutual contribution for exhibiting ferroelectricity as well as magnetism.

As known, ceramics are much more attractive due to their low cost, simpler, easy to control process parameters, and versatility. A systematic study has therefore been undertaken on the polycrystalline BTO substituted with different concentration of Zn and Mn at Ba and Ti site of BTO respectively. The main motivation of the present article is to understand the role of both Zn and Mn on the structural, electrical and magnetic properties of BTO. With an aim to induce magnetism especially in the promising ferroelectric BTO, we have co-substituted Zn and Mn at Ba and Ti sites respectively.

## 2 Experiment

### 2.1 Preparation

High-purity (99.99%) $BaCO_3$, $TiO_2$, $MnO_2$ and ZnO powders were taken and mixed according to the formula $Ba_{1-x}Zn_xTi_{1-x}Mn_xO_3$ (with $x$ = 0, 0.02, 0.04, 0.06, 0.08 and 0.1). Mixed powders were thoroughly ground and calcined in air at 950 ℃ for 24 h. Repeated quenching and grinding of the calcined powders were done for five times. Calcined powders were pressed (pressure of 10 T/cm$^2$) into pellets using poly vinyl alcohol (PVA) as binder. Pellets were sintered in tube furnace attached with programmable Eurotherm controller (Model: −2416) at 1300 ℃ for five hours.

### 2.2 Characterization

The sintered pellets were silver pasted for electrical measurement. X-ray diffraction (XRD) experiments were carried out on Bruker (D8) powder diffractometer (Cu Kα1 = 1.5406 Å) and the data refinement was performed with Rietveld method on FullProf software package. Scanning electron micrograph (SEM) studies were carried out on EVO-60 (ZEISS). The ferroelectric measurements were carried out with ferroelectric loop tracer (Precision Premier-II, Radiant). The magnetic measurements were performed using VSM (Lakeshore, model 7410). Chemical bonding analyses of sintered pellets were performed using XPS (VG system with a base pressure of $1\times10^{-10}$ Torr). All the above measurements were done at room temperature.

## 3 Results and discussion

Figure 1 shows the XRD patterns of $Ba_{1-x}Zn_xTi_{1-x}Mn_xO_3$ ceramics, where $x$=0, 0.02, 0.04, 0.06, 0.08 and 0.1. At the low doping levels ($x$=0.02), only diffraction peaks arising from tetragonal phase of $BaTiO_3$ (t-BTO) are observed. With increase in doping

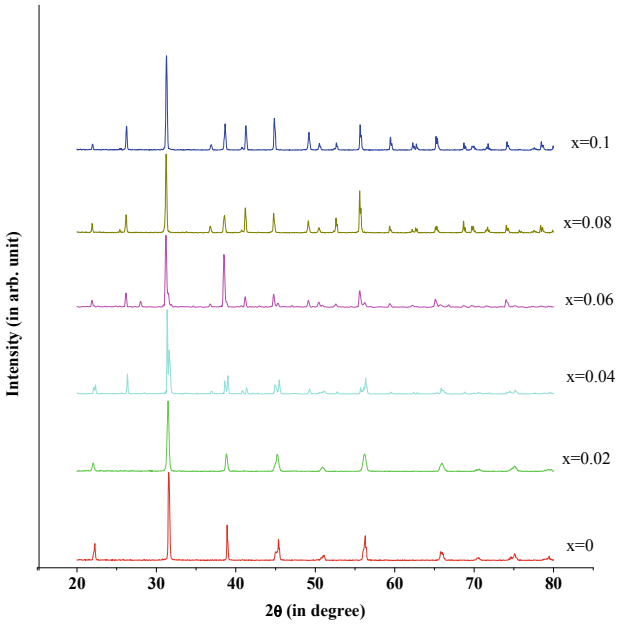


Fig. 1 X-ray diffraction (XRD) patterns of the compositions $Ba_{1-x}Zn_xTi_{1-x}Mn_xO_3$, where $x$=0, 0.02, 0.04, 0.06, 0.08, 0.1.

level ($x \geqslant 0.04$), additional diffraction peaks related to the hexagonal phase of $BaTiO_3$ (h-BTO) are appeared. When the value of '$x$' reaches 0.1, peaks associated with h-BTO phase are only visible. The lattice parameters of t-BTO are observed to be $a=b=3.996$ Å, $c=4.021$ Å & $\alpha=\beta=\gamma=90°$ with space group P4mm. However, the lattice parameters of $Ba_{0.9}Zn_{0.1}Ti_{0.9}Mn_{0.1}O_3$ are observed to be $a=b=5.719$ Å, $c=13.959$ Å & $\alpha=\beta=90°$, $\gamma=120°$ with space group $P6_3/mmc$.

The percentage (%) of tetragonal and hexagonal phases in Zn and Mn co-doped BTO ($Ba_{1-x}Zn_xTi_{1-x}Mn_xO_3$) with varying '$x$' from 0 to 0.1 are shown in Fig. 2. Percentage of each phase in all ceramic samples is calculated according to Andrei Kirianov's report [17]. It is clearly seen from Fig.2 that samples are only in tetragonal phase when '$x$' varies from 0 to 0.02. The hexagonal phase begins from $x$=0.04 and its proportion increases onward with reduction in the percentage of tetragonal phase. At $x$=0.1, the sample remains within the admixture of hexagonal phase with few fraction of tetragonal phase. Other researchers reported similar kinds of observations for Fe doped BTO [1]. The novelty of our equiproprotional co-doped is that bulk material showed both ferroelectric (lossy type) and ferromagnetic signature at $x$=0.1.

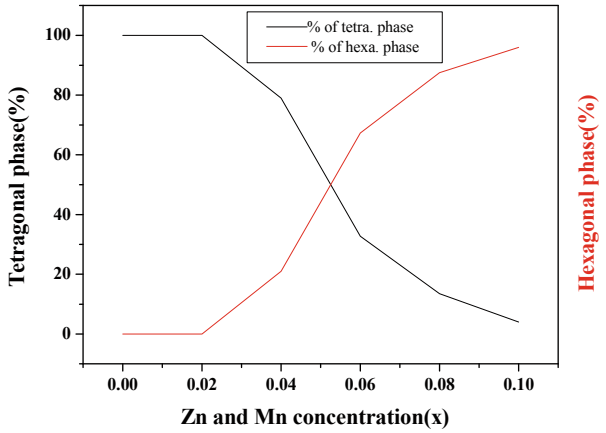


Fig. 2 Variation of tetragonal to hexagonal phases in the compositions $Ba_{1-x}Zn_xTi_{1-x}Mn_xO_3$ with the concentration ($x$) of Zn and Mn.

Figure 3 shows the Rietveld refinement of $BaTiO_3$ and $Ba_{0.9}Zn_{0.1}Ti_{0.9}Mn_{0.1}O_3$ samples. Details of refinement parameters are shown in the Table 1. There are generally two approaches for the stabilization of h-BTO. One approach is by doping of 3d ions such as Mn, Fe or Ni in oxidizing atmosphere [6,7]. The stabilization of hexagonal phase is reported to decrease the dielectric constant [6,16] and promotes exaggerated grain growth. Secondly, one can also stabilize h-BTO by heating under reducing atmosphere in pure hydrogen [14]. In our present case, we have developed h-BTO without processing the co-doped BTO under reducing or oxidizing atmosphere at high temperature (>1300 ℃). Hence, we conclude that apart from mono doped Mn in BTO, co-doped with Zn also responsible for the stabilization of h-BTO. When Mn atoms substitute at the Ti sites in the t-BTO, the atomic arrangement around Mn is distorted [14]. When the Mn concentration reaches the critical value, i.e. $x$=0.04, the structural transition to hexagonal phase takes place. On the other hand, the transformation from tetragonal phase to hexagonal one is also related to the concentration of equilibrium oxygen deficiency [9] or Jahn-Teller effect [7] induced by accepter dopants. $Ba_{1-x}Zn_xTi_{1-x}Mn_xO_3$ ceramics with a low-level of Mn concentration do not have much enough oxygen vacancies for the full transition from tetragonal phase to hexagonal one. With the increase in the Mn concentration, the amount of oxygen vacancies increases. More and more octahedrons convert from the corner-sharing structure to the face sharing one and hence the amount of the hexagonal phase increases.

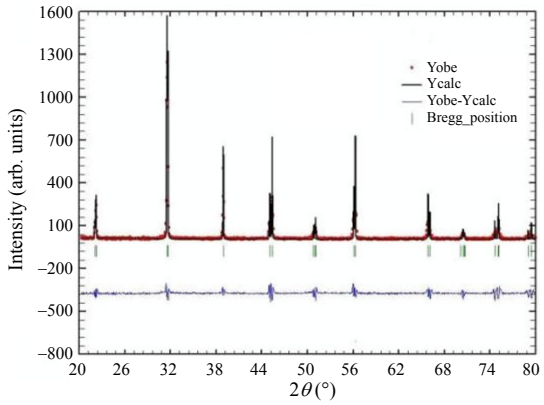


(a)

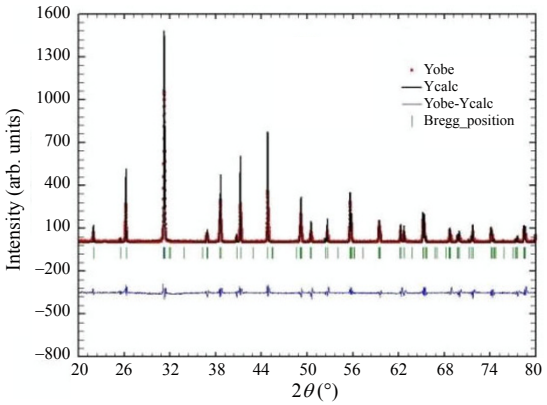


(b)

Fig. 3 Reitveld refinement of (a) $BaTiO_3$ and (b) $Ba_{0.9}Zn_{0.1}Ti_{0.9}Mn_{0.1}O_3$ ceramic samples.

Table 1 Rietveld refinement results of the ceramic samples $BaTiO_3$ and $Ba_{0.9}Zn_{0.1}Ti_{0.9}Mn_{0.1}O_3$

| Refined parameters | BaTiO3 | Ba0.9Zn0.1Ti0.9Mn0.1O3 |
|---|---|---|
| Volume (Å3) | 64.2100 | 395.430 |
| $R$-pattern ($R_p$) | 0.2670 | 0.2520 |
| $R$-weighted pattern ($R_{wp}$) | 0.2730 | 0.2880 |
| $R_{wp}$ expected ($R_{exp}$) | 0.2270 | 0.2160 |
| $R$-structure factor ($RF$) | 0.0135 | 0.0987 |
| Bragg $R$ factor | 0.0129 | 0.0642 |
| $S$ (goodness-of-fit) | 1.2000 | 1.3300 |

Here, $R_p=\Sigma\{y_i(o)-y_i(c)\}/\Sigma y_i(o)$, $R_{wp}=[\Sigma w_i\{y_i(o)-y_i(c)\}2/\Sigma w_i y_i(o)2]$, $R_{exp}=\{(N-P)/\Sigma w_i y_i(o)^2\}^{1/2}$, $S=R_{wp}/R_{exp}$ $y_i(o)$ and $y_i(c)$ are observed and calculated intensities at profile point $i$, respectively & $w_i$ is the weight for each Step $i$. $N$ and $P$ are number of experimental observations and the number of fitting parameters.

SEM studies were carried out for the compositions $Ba_{1-x}Zn_xTi_{1-x}Mn_xO_3$ (varying '$x$' values as $x$=0, 0.04, 0.06, 0.08, 0.1), which are shown in Fig 4. Figure 4a presents the SEM photograph of pure BTO sintered specimen. It is clearly enumerated from the photograph that pure BTO showed uniform grains and surface textures are appeared highly crystallize (Fig.1). With the increase of '$x$' values, i.e. $x$=0.04, it is clearly observed (Fig. 4b) that there is a significant grain growth which are homogenously distributed all over the surface leaving literally no room for micro pores or meso pores. However, with further increase of '$x$' from 0.04 to 0.06, SEM micrograph (Fig. 4c) showed the growth of crystallites with partial orientation. Directional grain growths of crystallites are also seen. With the increase of '$x$' from 0.08 to 0.1, a typical grain growth habits with rectangular cross sectional area are clearly seen. This grain growth habits are appeared to be inhomogeneous at $x$=0.08 (Fig. 4d). However, for $x$=0.1, (Fig. 4e), the micro crystallites with rectangular orientations are highly packed with homogeneous distributions. In fact, shape of micro crystallite and their distribution seen on the surface of the sintered specimen $x$=0.08 are composed of mainly two types of texture. One is rectangular and other is laminar. When $x$=0.1, mostly rectangular crystallites are seen as a measure surface texture along with less laminar plate-like texture as compared to $x$=0.08. It is argued that such kinds of micro structural difference with respect to their grain growth habits and distributions are dependent on the composition as well as percentage of the structural transformation from tetragonal to hexagonal phase. Our observation (Fig. 2) regarding the development of hexagonal phase from tetragonal phase promotes rectangular grain growth habits (Fig. 4e). It may be recalled that h-BTO phase at high temperature (>1300 ℃) either processed in

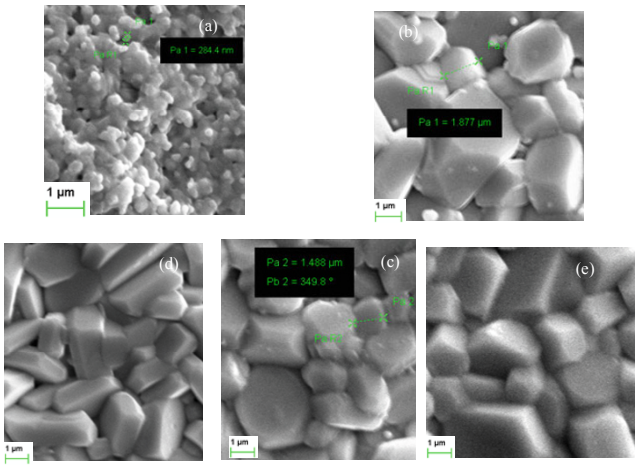


Fig. 4 SEM images of (a) BaTiO3, (b) $Ba_{0.96}Zn_{0.04}Ti_{0.96}Mn_{0.04}O_3$, (c) $Ba_{0.94}Zn_{0.06}Ti_{0.94}Mn_{0.06}O_3$, (d) $Ba_{0.92}Zn_{0.02}Ti_{0.92}Mn_{0.1}O_3$ and (e) $Ba_{0.9}Zn_{0.1}Ti_{0.9}Mn_{0.1}O_3$ samples.

oxidizing or reducing atmosphere, normally yield exaggerated grain growth. In our present work, we have not seen any exaggerated grains in hexagonal phase. Again, equiproprotional substitution of Zn and Mn in BTO is appeared essential for the formation of h-BTO. Grain sizes (from SEM photograph) of different compositions are given in Table 2. It is inferred here that micro structural grain growth habit and their distributions are completely dependent with the values of '*x*'.

To observe the oxidation state of the metal ions in the sintered sample, XPS studies were performed. Figure 5a shows the survey scan spectra of $Ba_{0.9}Zn_{0.1}Ti_{0.9}Mn_{0.1}O_3$. It is observed from Fig. 5b that the peak of Ba $3d_{5/2}$ is located at 782.59 eV instead of 779.6 eV of t-BTO [17], which shows the clear indication of structural transformation. Similarly, it is also observed from Fig. 5c that the Ti $2p_{3/2}$ peak is located at 461.40 eV instead of at 458.4 eV of t-BTO [17]. Generally, the magnitude of the binding energies is greater in h-BTO [18]. In hexagonal phase, the separation between the Ba-sites is generally much larger means the repulsion is minimized and results in a more negative binding energy [18]. The above two facts confirm the structural phase transition of BTO from tetragonal to hexagonal. It is also observed from XPS study that there is very low intensity of peaks of Zn (not shown), which indicate the low concentration of Zn present onto the surface of the sample. From the inset of Fig. 5c, it is elucidated that there is some multiplet splitting of Mn (3p) XPS spectra. As known, Mn can remain on the oxidation states ranging from $2^+$ to $7^+$ [11]. Hence, it indicates that Mn is in multiple oxidation state, which is likely to contribute the magnetic signature obtained at $x$=0.1.

The variations in the crystal structure, concentration of Mn and Zn dopants and defects such as oxygen vacancies [19] are strongly influenced the magnetic properties of $Ba_{1-x}Zn_xTi_{1-x}Mn_xO_3$ ceramics.

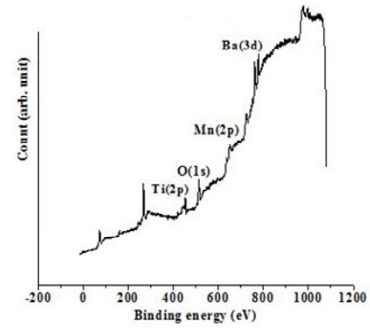


(a)

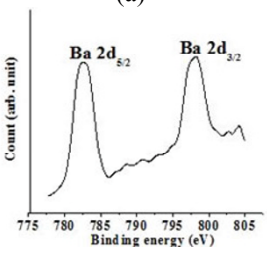


(b)

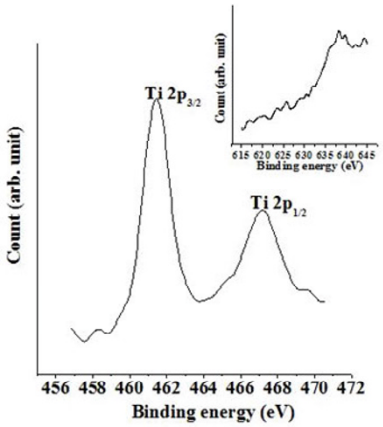


(c)

Fig. 5 (a) Survey scan spectra of the sample $Ba_{0.9}Zn_{0.1}Ti_{0.9}Mn_{0.1}O_3$, (b) XPS spectra of Ba, (c) XPS spectra of Ti and the inset of 5 (c) shows the XPS spectra of Mn.

Figure 6 shows the M-H curves of $Ba_{1-x}Zn_xTi_{1-x}Mn_xO_3$ and it is revealed that the whole M-H curve can be differentiated in to four regions, i.e., (i) $x$=0, (ii) $x$=0.02,

Table 2 Grain size, P-max and switching field for the compositions $Ba_{1-x}Zn_xTi_{1-x}Mn_xO_3$, where $x$=0, 0.02, 0.04, 0.06, 0.08, 0.1

| Compositions | approx. grain size | Max. polarization (P-max) in μC/cm$^2$ | Coercive field (Ec) in kV/cm |
|---|---|---|---|
| $BaTiO_3$ | 284.4 nm | 17.3 | 2.2 |
| $Ba_{0.98}Zn_{0.02}Ti_{0.98}Mn_{0.02}O_3$ | | 1.26 | 4.7 |
| $Ba_{0.96}Zn_{0.04}Ti_{0.96}Mn_{0.04}O_3$ | 1.8 μm | 1.18 | 4.2 |
| $Ba_{0.94}Zn_{0.06}Ti_{0.94}Mn_{0.06}O_3$ | 1.5 μm | 0.53 | 3.1 |
| $Ba_{0.92}Zn_{0.08}Ti_{0.92}Mn_{0.08}O_3$ | 2.2 μm | 0.28 | 4.9 |
| $Ba_{0.9}Zn_{0.1}Ti_{0.9}Mn_{0.1}O_3$ | 3.3 μm | 0.33 | 5.5 |

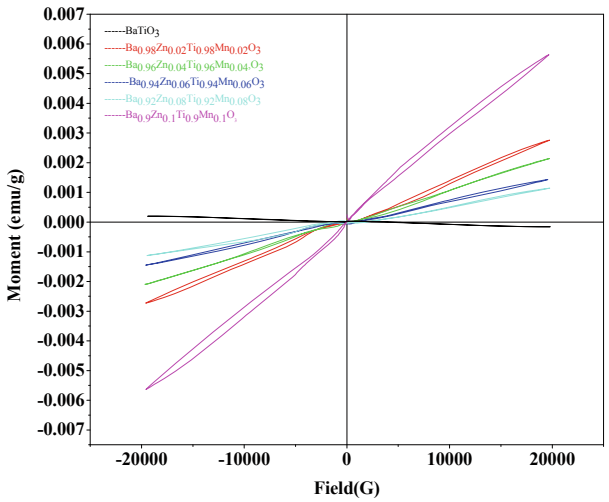


Fig. 6 Room temperature M~H loop of the compositions $Ba_{1-x}Zn_xTi_{1-x}Mn_xO_3$, where $x$=0, 0.02, 0.04, 0.06, 0.08, 0.1.

(iii) $x$=0.04, 0.06, 0.08 and, (iv) $x$=0.1. The ceramic shows the diamagnetic behaviour at $x$=0. For $x$=0.02, some narrow loop arises and the loop decrease with increase in '$x$' up to 0.08. After that at $x$=0.1, there is a drastic change in M-H loop. The magnetism at $x$=0.02 is likely to be related to intrinsic defects of oxygen vacancies and oxygen vacancies mediated coupling of Ti ions [19]. As we know, oxygen vacancies create spin polarization [19,20], which results exchange type interaction between Ti ions mediated by oxygen vacancies. The M-H curve of the samples $x$=0.04, 0.06, 0.08 are expected to be combinations of diamagnetic and paramagnetic (PM) parts. With increasing '$x$', the PM behavior decreases from 0.04 to 0.08. Here, the magnetic separation is associated with the crystalline volume fraction of the tetragonal and hexagonal phases as shown in Fig. 2. The decrease in the volume fraction of tetragonal phase reduces the PM order [1]. Further, with the increase of Mn concentration in the sample, the ferromagnetic oxygen vacancies mediated coupling could be collapsed by paramagnetic Mn ions incorporated randomly into BTO lattices and contribute to the peculiar M-H loop observed for $x$=0.04 to 0.08. Unsaturated double loop of the M-H curve (Fig. 6) for $x$=0.1 proves the coexistence of FM and anti-FM phases [1]. From XPS curve (inset of Fig. 5c), it is known that Mn exists in multiple oxidation state. As the ionic radius of $Mn^{3+}$ (low spin/ high spin) and $Mn^{4+}$ are 0.58 Å/0.645 Å and 0.53Å [14] respectively, which is comparable to the ionic radius of Ti. Hence, there is more possibility for the occurrence of $Mn^{3+}$ and $Mn^{4+}$ ions in the $x$=0.1 sample. As mentioned above, both ions $Mn^{3+}$ and $Mn^{4+}$ coexist in our system and therefore exchange interactions of $Mn^{3+}$-$Mn^{4+}$, $Mn^{3+}$-$Mn^{3+}$ and $Mn^{4+}$-$Mn^{4+}$ are possible [14]. In the hexagonal structure, the Mn ions can be located at the sites of pentahedral and octahedral [11]. The interactions of Mn ions between these two sites are responsible for the magnetic properties. These results noted to be consistent with the Dietl et al [21] model in which the net magnetization is given by the difference between the carrier-mediated ferromagnetism and the antiferromagnetic direct interactions between $Mn^{+}$ ions [22].

Figure 7 shows the P~E curves of $Ba_{1-x}Zn_xTi_{1-x}Mn_xO_3$ ceramics at room temperature. It is observed that with the increase of '$x$', the value of maximum polarization decreases as well as the area of the loop also decreases. The details of maximum polarization and coercive field ($E_c$) for each sample are shown in Table 2. The P~E loop observed for the samples with $x \geqslant 0.02$ (in Fig. 7) are typical of a lossy linear dielectric rather than for a ferroelectric material. This behavior suggests that either the doped ceramics are still in the sub-switching regime even at field of the order of 25 kV/cm or the ferroelectricity is largely suppressed. With increase in the concentration of Zn and Mn in BTO, the behavior of the ferroelectric loops changes noticeably and the maximum polarization (P-max) values have decreased from 17.3 μC/cm$^2$ (for t-BTO) to 0.33 μC/cm$^2$ (for $Ba_{0.9}Zn_{0.1}Ti_{0.9}Mn_{0.1}O_3$). This may be attributed to the formation of hexagonal phase. Since the hexagonal phase of BTO is not ferroelectric [9], the formation of the hexagonal phase weakens the ferroelectricity of $BaTiO_3$ to a large extent [9]. The stability of the ferroelectric phase can be determined by structural transition with additional factors like incorporation of foreign atoms [23]. It is evident that persistence of ferroelectricity results from the long-range polar orders of dipoles [24]. Any disruption in the polar order would affect the ferroelectricity. Generally, reduction of polarization occurs due to reduction in grain size [23], the presence of structural imperfections such as oxygen vacancies and dislocations [23]. It is also observed from Table 2 that the value of coercive field ($E_c$) remains high and the maximum polarization value reduces sharply ($P$-max) for all compositions. The above fact indicates that all the samples are highly insulator. Here, the reasons for degradation of ferroelectricity may be due to formation of hexagonal phase along with the creation of oxygen loss by co-substitution of Mn

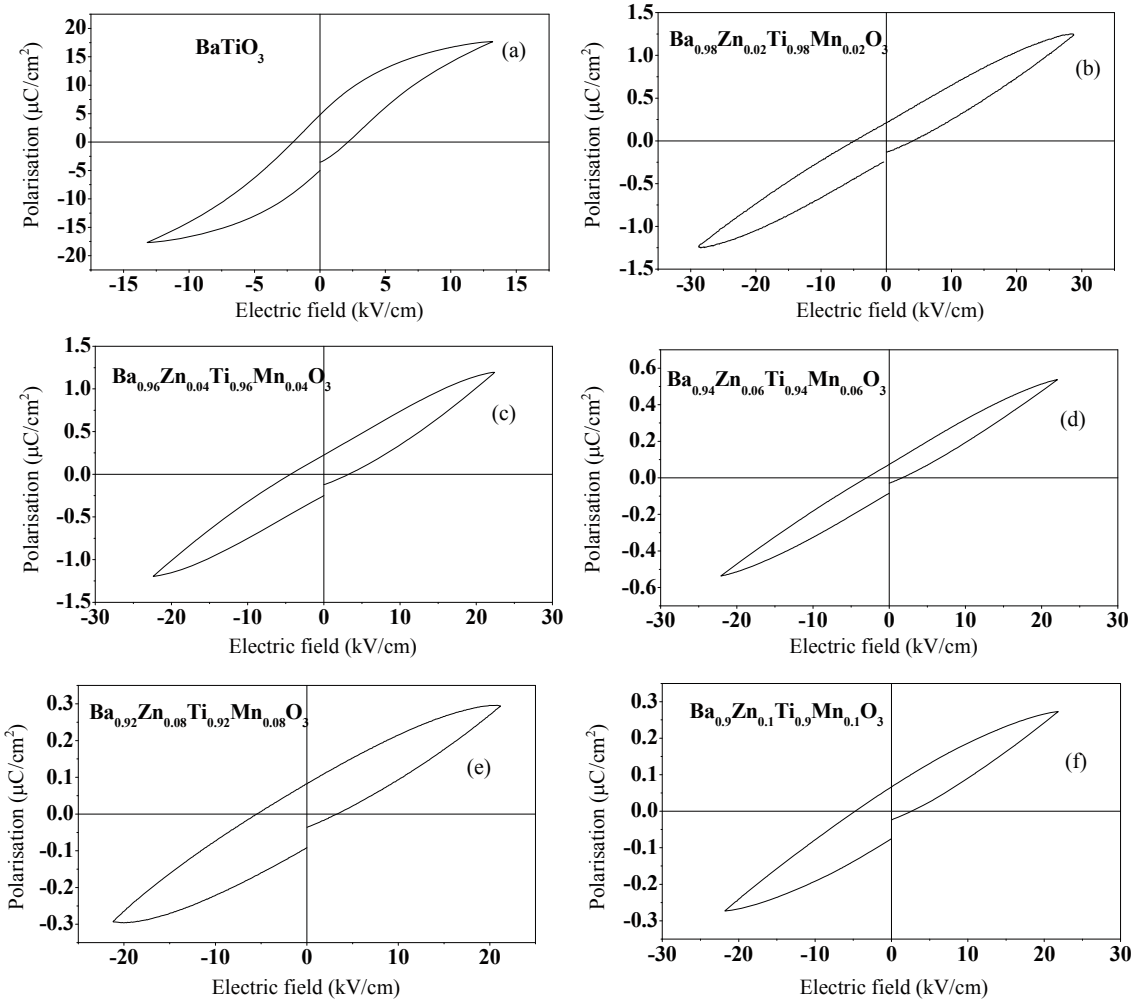


Fig. 7 Room temperature P ~E loop of (a) $BaTiO_3$, (b) $Ba_{0.98}Zn_{0.02}Ti_{0.98}Mn_{0.02}O_3$, (c) $Ba_{0.96}Zn_{0.04}Ti_{0.96}Mn_{0.04}O_3$, (d) $Ba_{0.94}Zn_{0.06}Ti_{0.94}Mn_{0.06}O_3$, (e) $Ba_{0.92}Zn_{0.02}Ti_{0.92}Mn_{0.1}O_3$, and (f) $Ba_{0.9}Zn_{0.1}Ti_{0.9}Mn_{0.1}O_3$ samples.

and Zn.

## 4 Conclusion

The structural, surface morphological, ferroelectric, and magnetic properties of $Ba_{1-x}Zn_xTi_{1-x}Mn_xO_3$ (where, $x$=0, 0.02, 0.04, 0.06, 0.08, 0.1) ceramics are investigated as functions of different concentration of Zn and Mn. Phase transformation from tetragonal to hexagonal of BTO ceramics are strongly influenced by the change of '$x$'. The hexagonal phase of BTO, which is generally a high temperature phase, is stabilised at room temperature by co-substituting of Mn and Zn. At $x$=0.1, the bulk sample showed both ferroelectric and ferromagnetic signature. Magnetism induced in this type ceramics are expected to be due to the defects such as the formation of oxygen vacancies and oxygen vacancies mediated spin polarisation. In addition to above, carrier induced exchange interactions between the different oxidation states of Mn are also likely to be responsible. Although the polarisation values are changed drastically, the coercive field remains high. It indicates the insulating nature of the ceramics. Present study clearly showed that magnetism especially ferromagnetism can be induced in a ferroelectric material by appropriate selection of substituents which may find multiferroic applications.

**Acknowledgement**

Author S. K. Das acknowledges to CSIR, New Delhi for providing financial support, CRF, IIT-Kharagpur for SEM measurements and CIF, IIT-Guwahati for magnetic

measurements. The authors also acknowledge to Mr. S. Choudhury of IOP, Bhubaneswar for his help in carrying out XPS measurements.

## References

[1] Dang NV, Thanh TD, Hong LV, *et al.* Structural, optical and magnetic properties of polycrystalline $BaTi_{1-x}Fe_xO_3$ ceramics. *J Appl Phys* 2011, **110**: 043-914.

[2] Shuai Y, Zhou S, Burger D, *et al.* Decisive role of oxygen vacancy in ferroelectric versus ferromagnetic Mn doped $BaTiO_3$ thin films. *J Appl Phys* 2011, **109**: 084-105.

[3] Tong X, Lin YH, Zhang S, *et al.* Preparation of Mn-doped $BaTiO_3$ nanoparticles and their magnetic properties. *J Appl Phys* 2008, **104**: 066-108.

[4] Nakayama H, Katayama-Yoshida H. Theoretical predication of magnetic properties of Ba $(Ti_{1-x}M_x)$ $O_3$ (M=Sc, V, Cr, Mn, Fe, Co, Ni, Cu). *Jpn J Appl Phys* 2001, **40**: 1355-1358.

[5] Chikada S, Hirose K, Yamamoto T. Analysis of local environment of Fe ions in hexagonal $BaTiO_3$. *Jpn J Appl Phys* 2010, **49**: 091-502.

[6] Phoosit N, Phanichphant S. Study on electrical properties of Mn-doped 6h-$BaTiO_3$ ceramics using impedance spectroscopy. *Chiang Mai J Sci* 2007, **34**(3): 297-308.

[7] Jayanthi S, Kutty TRN. Dielectric properties of 3d transition metal substituted $BaTiO_3$ ceramics containing the hexagonal phase formation. *J Mater Sci: Mater Electron* 2008, **19**: 615-626.

[8] Lin F, Shi W. Influence of non-isovalention substitution at A site on microstructure and magnetic properties of $Ba(Ti_{0.3}Fe_{0.7})O_3$ ceramic. *J Alloys Compd* 2010, **495**: 167-172.

[9] Du GP, Hu Z J, Han QF, *et al.* Effects of niobium donor doping on the phase structures and magnetic properties of Fe-doped $BaTiO_3$ ceramics. *J Alloys Compd* 2010, **492**: 79-81.

[10] Shuai Y, Zhou S, Schmidt H. Electrical and magnetic properties of polycrystalline Mn-doped $BaTiO_3$ thin films grown on Pt/sapphire substrates by pulsed laser deposition. *Advances in Sci and Tech* 2010, **67**: 212-217.

[11] Lin F, Shi W. Magnetic properties of transition-metal-codoped $BaTiO_3$ systems. *J Alloys Compd* 2009, **475**: 64-69.

[12] Gao L, Zhai J. The influence of Co doping on the dielectric, ferroelectric and ferromagnetic properties of $Ba_{0.70}Sr_{0.30}TiO_3$ thin films. *Applied Surface Science* 2009, **255**: 4521-4525.

[13] Fasaso AY, Maaza M, Rohwer EG, *et al.* Effect of Zn-doping on the structural and optical properties of $BaTiO_3$ thin films grown by pulsed laser deposition. *Thin Solid Film* 2008, **516**: 6226-6232.

[14] Kirianov A, Ozaki N, Ohsato H, *et al.* Studies on the solid solution of Mn in $BaTiO_3$. *Jpn J Appl Phys* 2001, **40**: 5619-5623.

[15] Miura K, Azuma M, Funakubo H. Electronic and structural properties of $ABO_3$: Role of the B-O coulomb repulsions for eerroelectricity. *Materials* 2011, **4**: 260-273.

[16] Langhammer HT, Muller T, Felgner KL, *et al.* Crystal structure and related properties of manganese-doped barium titanate ceramics. *J Am Ceram Soc* 2000, **83**: 605-611.

[17] Makhova L, Hesse R, Ullrich M, *et al.* Surface potential of $BaTiO_3$ single crystal near the Curie temperature. *Phys Rev B* 2011, **83**: 115-407.

[18] Dawson JA, Freeman CL, Ben LB, *et al.* An atomistic study into the defect chemistry of hexagonal barium titanate. *J Appl Phys* 2011, **109**: 084-102.

[19] Fang Y, KuiJuan J, HuiBin LU, *et al.* Oxygen vacancy induced magnetism in $BaTiO_{3-\delta}$ and Nb: $BaTiO_{3-\delta}$ thin films. *Science China* 2010, **53**: 852-855.

[20] Mangalama RVK, Ray N, Waghmare UV. Multiferroic properties of nanocrystalline $BaTiO_3$. *Solid State Commun* 2009, **149**: 1-5.

[21] Dietl T, Ohno H, Matsukura F. Zener model description of ferromagnetism in zinc-blende magnetic semiconductors. *Science* 2000, **287**: 1019-1022.

[22] Norton DP, Theodoropoulou NA, Hebard AF, *et al.* Properties of Mn-implanted $BaTiO_3$, $SrTiO_3$, and $KTaO_3$. *Electrochemical and Solid-State Letters* 2003, **6**: 19-21.

[23] Zhao Z, Buscaglia V, Viviani M, *et al*. Grain-size effects on the ferroelectric behavior of dense nanocrystalline $BaTiO_3$ ceramics. *Phys Rev B* 2004, **70**: 024-107.

[24] Kuehn M, Kliem H. The method of local fields: A bridge between molecular modelling and dielectric theory. *J of Elctrostatics* 2009, **67**: 203-208.